Intermetallic Compounds

DOI: 10.1002/anie.201203787

Isolated Pd Sites on the Intermetallic PdGa(111) and PdGa($\bar{1}\bar{1}\bar{1}$) Model Catalyst Surfaces**

*Jan Prinz, Roberto Gaspari, Carlo A. Pignedoli, Jochen Vogt, Peter Gille, Marc Armbrüster, Harald Brune, Oliver Gröning, Daniele Passerone, and Roland Widmer**

Catalytic reactions are of highest technological and economic importance, especially in the field of chemical synthesis and exhaust gas treatment.[1] About 80% of the reactions in chemical industry rely on catalysts, thus giving motivation for research in this area.[2,3] There has been enormous progress in heterogeneous catalysis through the understanding of reaction mechanisms and the relation of catalyst surface structures to the reaction rate and selectivity.[3–7] A major step forward has been achieved by comparing single-crystal model catalysts to real catalysts and by combining the ultrahigh-vacuum (UHV) surface-science approach with high-pressure studies of the reaction kinetics.[2–4] This development has led to a paradigm shift in catalyst development.[8]

Amongst the most ingenious and innovative catalyst materials are intermetallic compounds (IMCs) as they enable spatial separation of the catalytically active sites[9] and thus the achievement of both high activity and selectivity.[10] Additionally, it is also possible to tune the electronic properties of IMCs by changing their chemical composition. Recent results revealed that this new class of catalytic materials might be of industrial relevance, and outperform known catalysts, especially when highly selective processes are demanded.[11]

[*] J. Prinz,[+] Dr. R. Gaspari,[+] Dr. C. A. Pignedoli, Dr. O. Gröning, Dr. D. Passerone, Dr. R. Widmer
Empa. Swiss Federal Laboratories for Materials Science and Technology
Überlandstrasse 129, 8600 Dübendorf (Switzerland)
E-mail: roland.widmer@empa.ch
Homepage: http://www.surfaces.ch
Dr. J. Vogt
Chemisches Institut, Otto-von-Guericke-Universität
39106 Magdeburg (Germany)
Prof. Dr. P. Gille
Dept. für Geo- und Umweltwissenschaften
Ludwig-Maximilians-Universität, 80333 München (Germany)
Dr. M. Armbrüster
Max-Planck-Institut für Chemische Physik fester Stoffe
01187 Dresden (Germany)
J. Prinz,[+] Prof. Dr. H. Brune
Institute of Condensed Matter Physics, EPFL, Station 3
1015 Lausanne (Switzerland)
[+] These authors contributed equally to this work.

[**] This work was supported by the Swiss National Science Foundation under the contract 200021-129511. We kindly acknowledge D. Rosenthal, R. Schlögl (FHI Berlin), and Y. Grin (MPI Dresden) for fruitful discussions, and the Swiss Supercomputing Center (CSCS) for computational resources.

Supporting information for this article is available on the WWW under http://dx.doi.org/10.1002/anie.201203787.

PdGa IMCs have shown remarkable catalytic properties for an important reaction in polyethylene production, namely the partial hydrogenation of acetylene to ethylene.[11,13–15] However, the reaction pathway is largely unknown. We address this question on single-crystal IMC PdGa model systems.[4] Their bulk crystal and electronic structure have been reported earlier.[11–14,16–18] Herein, we determine and explore the stable surface terminations because they define the activity and selectivity of the catalyst.[8]

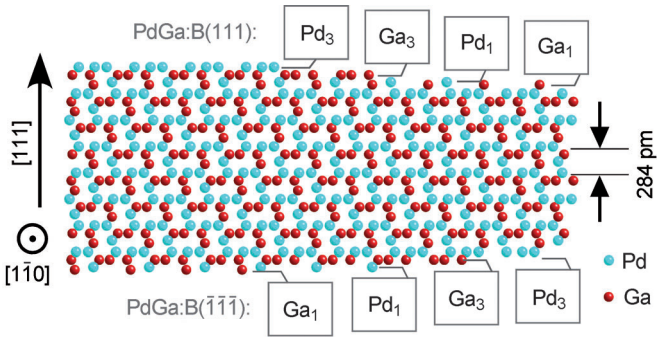

Figure 1. Bulk-truncated surface terminations of the PdGa:B(111) and ($\bar{1}\bar{1}\bar{1}$) surfaces. The surfaces are named according to Ref. [12], including the chemical composition, the enantiomeric form, and the surface direction.

We combine quantitative low-energy electron diffraction (LEED), high-resolution scanning tunneling microscopy (STM), and ab initio thermodynamics calculations to unequivocally identify the surface terminations of PdGa(111) and PdGa($\bar{1}\bar{1}\bar{1}$) surfaces. These surfaces exhibit significant differences in catalytic activity that are exemplified by calculations of hydrogen dissociation.

The crystal structure of PdGa belongs to the $P2_13$ space group and therefore exhibits two enantiomeric forms (labeled A and B in Refs. [12,19]). Figure 1 displays a side view onto a (1$\bar{1}$0) surface of the structure model of form B that was derived from X-ray diffraction.[16] The stacking sequence involves four nonequivalent atomic planes. As a consequence, the top and bottom surfaces are different, and each can exhibit four possible terminations. Recent STM investigations[12] revealed that there is only one step height, and its value of 284 pm corresponds to four atomic planes, thus implying that only one of the four terminations is realized. LEED and X-ray photoelectron diffraction have shown that the surfaces are chiral and unreconstructed.[12] Herein, we identify which of the four bulk terminations is realized and discuss the structure–reactivity relation.

Our initial approach to determining the surface terminations was by using LEED. This technique is intrinsically surface sensitive because of the small mean-free path of low-energy electrons. In addition to the diffraction images of the surface unit cells, information on the vertical structure was acquired from the variation of the diffraction spot intensities with incident electron energy owing to the interference of electrons scattered from lower-lying layers. Comparison of these *I–V* curves with simulated ones allows the determination of the atomic positions of the first atomic layers. The quality of this comparison is quantified by the Pendry reliability factor R_P[20] which is 0 for perfect agreement and 1 for uncorrelated profiles. The agreement is acceptable when R_P is less than 0.3.[20,21]

We compared experimental results to the theoretical results for the 32 possible structures that result from both enantiomeric forms of the crystal, the four bulk truncations, the two nonequivalent close-packed surfaces, that is, (111) and $(\bar{1}\bar{1}\bar{1})$, and both possible in-plane orientations of the sample. Density functional theory (DFT) was used to compute the atomic positions of the relaxed bulk-surface terminations. The SATLEED code was applied to calculate the LEED curves from these model structures.[21,22] The atomic positions were further fine-tuned to minimize the R_P factor for a given termination. The R_P factors for the model structures that were closest to the experimental structures are presented in Figure 2. The best fit was found for the PdGa:B(111)Pd_3 and PdGa:B$(\bar{1}\bar{1}\bar{1})Pd_1$ surface structures of the respective samples.

The difference in the R_P factor between the proposed structures is larger for the (111) surface than for the $(\bar{1}\bar{1}\bar{1})$ surface because of the much lower atomic density of the latter, and the weaker scattering cross section when Pd_1 terminated. Nevertheless, the difference remains significant also in that case, and the best fit for both structures give $R_p = 0.22$. To get an impression of the agreement between experimental and theoretical results, in Figure 2 we show for each surface the *I–V* curves for the structures with the lowest and highest R_p factors. Notably, the atomic displacements from the DFT relaxed structure that was used for the

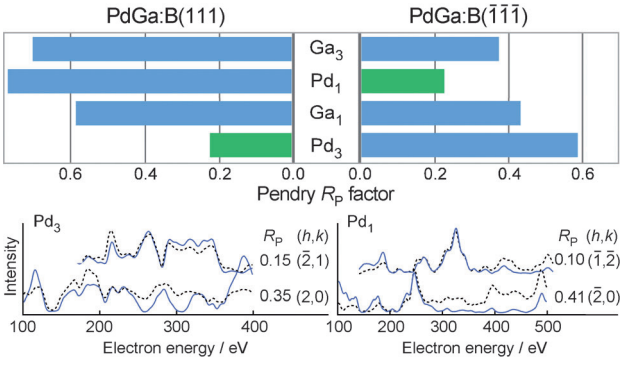

Figure 2. Top: R_P factors for the surface terminations that are shown in Figure 1. The experimental *I–V* data is derived from an average of 12 nonequivalent diffraction spots for each sample. The terminations giving best agreement are marked in green. Bottom: Experimental (dashed black line) and theoretical *I–V* curves (full blue line) for the two spot profiles that are in best and worst agreement among those of Pd_3 and Pd_1 (see also the Supporting Information).

optimization of the R_p factor are very small, being less than 7 pm in the vertical and less than 27 pm in the lateral direction. Finally, our LEED patterns confirm the formerly found absence of a surface reconstruction.[12]

The surface terminations found by LEED are confirmed by the atomic resolution STM images shown in Figure 3. The unit cells are imaged as a trimer for the (111) surface and as a single atomic protrusion for the $(\bar{1}\bar{1}\bar{1})$ surface. In both cases,

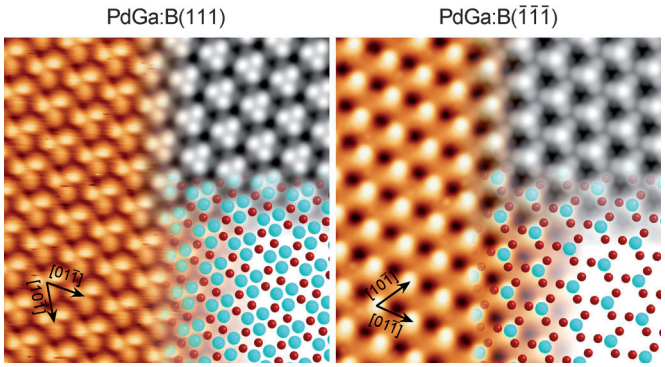

Figure 3. Atomically resolved STM images ($T = 77$ K) overlaid with simulated STM images (top right inset) and the respective structure models (bottom right inset; Pd = aqua, Ga = red). STM parameters (PdGa:B(111)Pd_3)/(PdGa:B$(\bar{1}\bar{1}\bar{1})Pd_1$): $V_T = 80/100$ mV; $I_T = 0.73/0.4$ nA; $\Delta z = 32/51$ pm; scan size = 6×6 nm^2.

the periodicity corresponds to the bulk value of 0.693 nm.[16] This atomic contrast was found for all terraces of the respective surfaces, thus confirming that only one stable termination exists. The STM simulations shown in the top right insets agree with the experimental results. These simulations were obtained by applying the Tersoff-Hamann (TH) formalism[23] to the DFT computed local density of states (LDOS; see the Supporting Information), the isovalue of which is matched to give good agreement with the experiment.

We addressed the physical origin of the stability of the identified terminations with DFT calculations. The relative stability of all PdGa terminations were computed in the grand canonical ensemble, where the different surfaces are at equilibrium with external sources of Pd and Ga atoms, and the equilibrium state is determined by the minimum of the Gibbs surface energy, G_s. The chemical potentials of the Pd and Ga atoms, μ_{Pd} and μ_{Ga}, depend on external parameters, such as pressure and temperature, and their individual values are generally unknown. However, the range of allowed μ_{Pd} and μ_{Ga} values can be determined by thermodynamic considerations.[24] The upper limit of the chemical potential of Pd and Ga in the alloy is given by the respective bulk values. Moreover, when the sources of Pd and Ga atoms are in equilibrium with the PdGa bulk, μ_{PdGa} is a function of μ_{Pd} and μ_{Ga}. This gives an interval of [Eq. 1]:

$$\mu_{Ga}^{bulk} + \frac{\Delta H_f}{4} \le \mu_{Ga} \le \mu_{Ga}^{bulk}$$
$$\mu_{Pd}^{bulk} + \frac{\Delta H_f}{4} \le \mu_{Pd} \le \mu_{Pd}^{bulk} \quad (1)$$

where ΔH_f is the enthalpy of formation of PdGa per unit cell, containing four Pd and four Ga atoms. For the bulk cohesive energies we find $\mu_{Pd}^{bulk} = -3.69$ eV and $\mu_{Ga}^{bulk} = -2.78$ eV, which are in agreement with previous results.[25,26] For the heat of formation per PdGa unit cell we obtain $\Delta H_f = -5.48$ eV, which is close to the experimental value of -5.96 eV.[27]

For both surface orientations, Figure 4 displays the resulting $\Delta G_s(\mu_{Ga})$ curves, computed using periodic slab calculations.[28] ΔG_s is expressed relative to PdGa:B(111)Ga_3

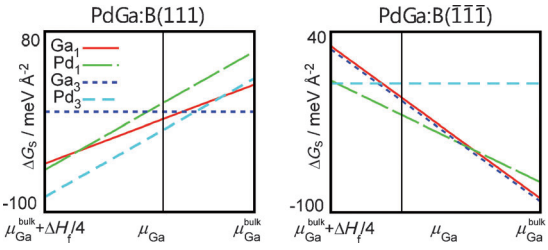

Figure 4. Change in Gibbs surface energy as a function of μ_{Ga} for the different terminations. Vertical lines refer to the actual value of the surface chemical potential estimated for the respective PdGa surfaces.

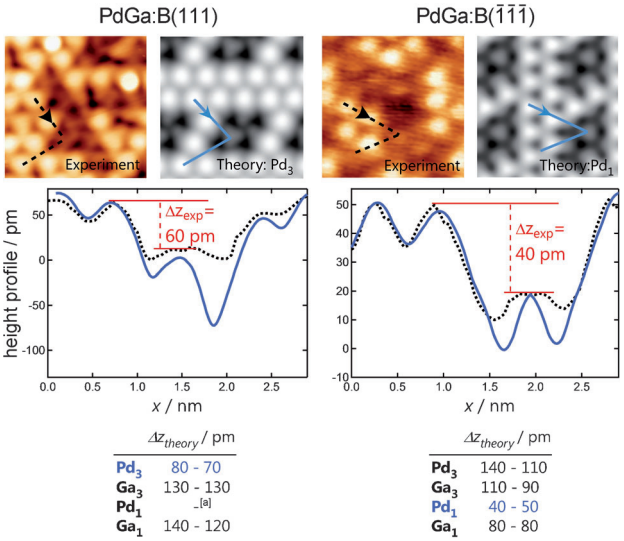

Figure 5. Top: Measured and calculated constant-current STM images. Middle: Apparent height profiles for experimental (dashed black line) and simulated (full blue line) STM images of surface vacancies. Bottom: The tables show simulated values of the apparent vacancy depths (Δz) for all DFT relaxed model terminations. The values that have best agreement between simulation and experiment are marked in blue. [a] In the DFT-optimized structure for (111)Pd_1 the underlying Ga layer relaxes towards the surface and becomes the top layer.

and PdGa:B$(\bar{1}\bar{1}\bar{1})Pd_3$, respectively (see the Supporting Information). The graphs shown reveal which surfaces can be expected over the whole range of external parameters. Clearly, the surface terminations determined by experiment have the widest stability ranges with a $\Delta\mu_{Ga}$ value of 1 eV and 0.8 eV in the two cases. This finding confirms the experimental results for both surfaces. Moreover, the actual values of the chemical potentials can be estimated under the assumptions that the Pd and Ga sources are in equilibrium with kink sites of the crystal surface and that the two opposite surfaces of the same sample equilibrate independently. The explicit calculation (see the Supporting Information) gives values of $\mu_{Ga}^{(111)} = \mu_{Ga}^{bulk} - 0.57$ eV and $\mu_{Ga}^{(\bar{1}\bar{1}\bar{1})} = \mu_{Ga}^{bulk} - 0.90$ eV, which are indicated in the energy profiles (Figure 4) as vertical lines. Again, for these specific values $Pd_3(111)$ and $Pd_1(\bar{1}\bar{1}\bar{1})$ are found to be the most stable terminations, in agreement with the experimental results.

STM images of surface vacancies provide an additional and very sensitive test of the determined surface terminations. The distance from the surface as well as the chemical composition of the underlying layer varies strongly with the surface termination, thus giving rise to termination specific STM contrast between the surface and vacancies. Figure 5 shows a comparison of measured and calculated constant-current STM images and apparent height profiles going from regular surface areas to vacancies and back. The surface layer is identified from the simulated STM vacancy profiles for all bulk terminations, by comparison of the calculated vacancy depths with the experimental value.

For both surfaces, the measured apparent-vacancy heights agree well with the calculated ones for the two identified terminations, and differ significantly from all other terminations. This result gives us additional confidence that PdGa:B(111)Pd_3 and PdGa:B$(\bar{1}\bar{1}\bar{1})Pd_1$ are the actual surface structures. The STM simulations were obtained using the TH[23] model and DFT relaxed surface structures displaying patterns of 2×2 vacancies with monoatomic steps. The comparison of experimental and theoretical results is particularly robust, as the vacancy depth is rather stable against changes of simulated isocurrent or tip radius. A large range of tip–sample distances was covered by simulating STM images for integrated LDOS values of 10^{-7} and 10^{-11} e Å^3. For a pointlike tip, these values correspond to tip–sample distances of 0.45 nm and 0.9 nm, respectively. The vacancy depth intervals given in Figure 5 come from these two extreme tip–sample distances and provide a conservative error margin of the STM simulation.

An initial indication of the catalytic activity of the two surface terminations can be obtained from the position of the metal d-band center with respect to E_F, an indicator for the bonding strength of adsorbates to metallic surfaces.[29] However, this simple d-band-center rule has to be taken with care, both, because covalent bonding plays a role in this system, and in case molecular adsorption modifies considerably the band shape (as seen in the Supporting Information, this is the case for hydrogen adsorption).[30] For high catalytic activity, the bond to a reactant molecule should be of intermediate strength, this is known as the Sabatier principle.[31] In comparison to Pd(111), (for details see the Supporting Information) the Pd d-band edge of both PdGa surfaces is found at lower energy, which is an indication (with the above caveats) of a weaker binding of the adsorbed molecules on the IMC surfaces, in agreement with thermal desorption spectroscopy (TDS) results.[12] Additionally, the PdGa surfaces exhibit a sharper d-band, and thus a stronger localization of electronic states. In spite of their electronic similarity, as seen

by the projected density of states (pDOS; see the Supporting Information), the two PdGa terminations allow for different adsorption conformations as single Pd atoms or Pd trimers terminate the surface. This site separation is particularly evident for Pd_1, where the surface atomic Pd–Pd distance is 2.5 times larger than for Pd(111), and more than twice the bulk value of PdGa.[14]

A more elaborate assessment of the catalytic properties can be obtained by DFT calculations of the binding energies and adsorption sites; we performed these calculations for molecular and atomic hydrogen adsorbed onto both surfaces (Figure 6) while no hydrogen uptake into the bulk is expected.[32] On PdGa:B$(\bar{1}\bar{1}\bar{1})$Pd$_1$ the most favorable adsorption site for H_2 is the Pd_1 on-top position with an adsorption energy of 0.22 eV per H_2 molecule. From this site H_2 dissociation is exothermic with 0.11 eV and the most favorable site for atomic hydrogen is the threefold coordinated hollow site on the Pd_3 trimer (Figure 6, right). This position is 70 pm below the Pd_1 surface plane, and 13 pm below the first Ga_3 plane, a site that is sufficiently close to the surface for the adsorbate to remain available for the hydrogenation of other molecules.

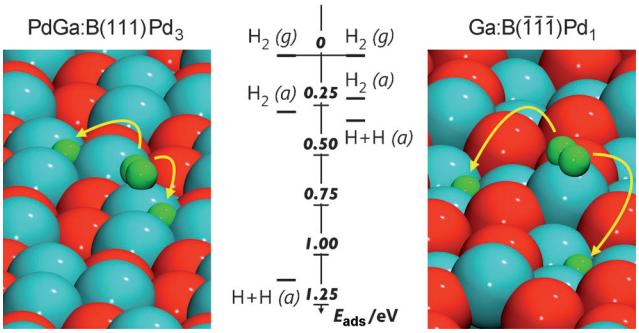

Figure 6. Adsorption sites and binding energies for H_2 and H on the investigated surfaces. Energies are given in eV per H atom couple with respect to the molecule in the gas phase.

The adsorption energy of H_2 on PdGa:B(111)Pd$_3$ is 0.28 eV, and thus comparable to PdGa:B$(\bar{1}\bar{1}\bar{1})$Pd$_1$. Furthermore, similar adsorption positions for H_2 and H are identified for both surfaces, that is, Pd top site and Pd threefold hollow site, respectively. However, H_2 dissociation is associated with a larger energy gain of 0.85 eV on the Pd_3 termination. This comparison reveals that both surface orientations with their terminations determined in the present study show mostly quantitative differences in their behavior towards H_2 dissociation. Although the binding energies of the molecular precursor are quite similar, one surface has more strongly bound dissociation products than the other. The different bonding mechanisms of both surfaces are also highlighted by the projected densities of states. Hybridization of the H s level with the Pd d bands shows a different fine structure at around 6 eV below the Fermi energy (see the Supporting Information), which is where there is maximum overlap between H and Pd orbitals participating in the bonding (as it results from a bond-order analysis performed within Bader's topological theory of atoms in molecules,[33] see Supporting Information. This analysis also confirms the stronger bonding of H atoms on the surface trimer on the PdGa:B(111)Pd$_3$).

In conclusion, we have determined the surface terminations of the IMC PdGa:B(111)Pd$_3$ and PdGa:B$(\bar{1}\bar{1}\bar{1})$Pd$_1$. The structural details revealed in this work and their implications on the binding of adsorbates will serve as the essential basis for understanding chemical reactions on the PdGa surfaces and help develop high performance catalysts from intermetallic compounds. The structural dissimilarities of the two surface terminations lead to significant energetic differences in the catalytic dissociation of a molecule as simple as hydrogen, an essential reagent in many relevant reactions. We expect similar or even larger differences for organic molecules, a topic to be addressed in a forthcoming publication. Moreover, the structural dissimilarity of the (111) and $(\bar{1}\bar{1}\bar{1})$ surfaces makes the IMC PdGa a prototype model system, which allows the study of the effect of active-site separation in heterogeneous catalysis.

Experimental Section

Methods: The single-crystal samples used in this study originate from one large PdGa crystal grown by the Czochralski method.[34] After cutting and polishing, reflective energy dispersive X-ray diffraction determined the surface orientations to be within 0.3° precise.

STM measurements were performed with an Omicron low-temperature STM at 77 K and at a base pressure below 5×10^{-11} mbar with a mechanically cut Pt/Ir-tip. STM data were analyzed using the WSxM software.[35]

Sample preparation in UHV consists of several sputter-annealing cycles (sputtering: Ar^+, 1 keV; annealing: 20 min at 870 K) until a sharp (1×1) LEED pattern was obtained. During preparation, no change in the surface stoichiometry of PdGa was observed.[12] The LEED investigations were carried out with an Omicron multichannelplate Specta-LEED and acquired with a CCD camera at 1 eV/frame. Video analysis was performed using the Spectaview software from Omicron. *I–V* profiles for the single spots were background corrected. The angle of incidence was perpendicular to the surface, thus allowing for averaging over the symmetry equivalent spot profiles leading to an improved signal to noise ratio.[21–22]

Relative surface energies have been computed using DFT slab calculations, employing the PWSCF[36] code. Simulated STM vacancy heights have been computed using supercell DFT slab calculations employing the CP2K[37] code (for further details see the Supporting Information).

Received: May 16, 2012
Revised: June 8, 2012
Published online: August 22, 2012

Keywords: density functional calculations · electron diffraction · heterogeneous catalysis · intermetallic compounds · surface chemistry

[1] U. Dingerdissen, A. Martin, D. Herein, H. J. Wernicke in *Handbook of Heterogeneous Catalysis* (Eds.: G. Ertl, H. Knözinger, F. Schüth, J. Weitkamp), VCH, Weinheim, **2008**.
[2] J. A. Dumesic, G. W. Huber, M. Boudart in *Handbook of Heterogeneous Catalysis* (Eds.: G. Ertl, H. Knözinger, F. Schüth, J. Weitkamp), VHC, Weinheim, **2008**.

[3] G. Kyriakou, M. B. Boucher, A. D. Jewell, E. A. Lewis, T. J. Lawton, A. E. Baber, H. L. Tierney, M. Flytzani-Stephanopoulos, E. C. H. Sykes, *Science* **2012**, *335*, 1209 – 1212.
[4] G. A. Somorjai, *Science* **1985**, *227*, 902 – 908.
[5] H. J. Freund, N. Ernst, T. Risse, H. Hamann, G. Rupprechter, *Phys. Status Solidi A* **2001**, *187*, 257 – 274.
[6] G. Ertl, H. J. Freund, *Phys. Today* **1999**, *52*, 32 – 38.
[7] M. Ortega Lorenzo, C. J. Baddeley, C. Muryn, R. Raval, *Nature* **2000**, *404*, 376 – 379.
[8] J. K. Nørskov, T. Bligaard, J. Rossmeisl, C. H. Christensen, *Nat. Chem.* **2009**, *1*, 37 – 46.
[9] W. M. H. Sachtler, *Catal. Rev. Sci. Eng.* **1976**, *14*, 193 – 210.
[10] M. Armbrüster in *Encyclopedia of Catalysis* (Ed.: I. T. Horvath), VCH, Weinheim, **2011**.
[11] J. Osswald, K. Kovnir, M. Armbrüster, R. Giedigleit, R. E. Jentoft, U. Wild, Y. Grin, R. Schlögl, *J. Catal.* **2008**, *258*, 219 – 227.
[12] D. Rosenthal, R. Widmer, R. Wagner, P. Gille, M. Armbrüster, Y. Grin, R. Schlögl, O. Gröning, *Langmuir* **2012**, *28*, 6848 – 6856.
[13] J. Osswald, R. Giedigkeit, R. E. Jentoft, M. Armbrüster, F. Girgsdies, K. Kovnir, T. Ressler, Y. Grin, R. Schlögl, *J. Catal.* **2008**, *258*, 210 – 218.
[14] K. Kovnir, M. Armbrüster, D. Teschner, T. V. Venkov, F. C. Jentoft, A. Knop-Gericke, Y. Grin, R. Schlögl, *Sci. Technol. Adv. Mater.* **2007**, *8*, 420 – 427.
[15] M. Armbrüster, K. Kovnir, M. Behrens, D. Teschner, Y. Grin, R. Schlögl, *J. Am. Chem. Soc.* **2010**, *132*, 14745 – 14747.
[16] M. Armbrüster, H. Borrmann, M. Wedel, Y. Prots, R. Giedigkeit, P. Gille, *Z. Kristallogr. New Cryst. Struct.* **2010**, *225*, 617 – 618 (please consider the accidental interchanging of crystal form "A" and "B" in this reference).
[17] B. H. Verbeek, P. K. Larsen, W. M. Gerits, *Vacuum* **1983**, *33*, 813 – 814.
[18] K. Kovnir, M. Armbrüster, D. Teschner, T. V. Venkov, L. Szentmiklosi, F. C. Jentoft, A. Knop-Gericke, Y. Grin, R. Schlögl, *Surf. Sci.* **2009**, *603*, 1784 – 1792.
[19] J. C. H. Spence, J. M. Zuo, M. Okeeffe, K. Marthinsen, R. Hoier, *Acta Crystallogr. Sect. A* **1994**, *50*, 647 – 650.
[20] J. B. Pendry, *J. Phys. C* **1980**, *13*, 937 – 944.
[21] M. A. Van Hove, W. H. Weinberg, C. M. Chan, *Low-Energy Electron Diffraction*, Springer, Heidelberg, **1986**.
[22] A. Barbieri, M. A. Van Hove, private communication (http://www.ap.cityu.edu.hk/personal-website/Van-Hove.htm) ed.
[23] J. Tersoff, D. R. Hamann, *Phys. Rev. B: Condens. Matter Mater. Phys.* **1985**, *31*, 805 – 813.
[24] G. X. Qian, R. M. Martin, D. J. Chadi, *Phys. Rev. B: Condens. Matter Mater. Phys.* **1988**, *38*, 7649 – 7663.
[25] D. D. Wagman, W. H. Evans, V. B. Parker, R. H. Schumm, I. Halow, S. M. Bailey, K. L. Churney, R. L. Nuttall, *J. Phys. Chem. Ref. Data* **1982**, *11*, 1 – 405.
[26] C. Kittel, *Introduction to Solid State Physics*, Wiley, New York, **1971**.
[27] S. V. Meschel, O. J. Kleppa, *Thermochim. Acta* **1997**, *292*, 13 – 17.
[28] W. E. Pickett, *Comput. Phys. Rep.* **1989**, *9*, 115 – 197.
[29] B. Hammer, J. K. Norskov, *Surf. Sci.* **1995**, *343*, 211 – 220.
[30] A. Roudgar, A. Gross, *J. Electroanal. Chem.* **2003**, *548*, 121 – 130.
[31] P. Sabatier, *Ber. Dtsch. Chem. Ges.* **1911**, *44*, 1984 – 2001.
[32] M. Klanjsek, et al., *J. Phys.: Condens. Matter* **2012**, *24*, 085703.
[33] J. G. Angyan, M. Loos, I. Mayer, *J. Phys. Chem.* **1994**, *98*, 5244 – 5248.
[34] P. Gille, T. Ziemer, M. Schmidt, K. Kovnir, U. Burkhardt, M. Armbrüster, *Intermetallics* **2010**, *18*, 1663 – 1668.
[35] I. Horcas, R. Fernandez, J. M. Gomez-Rodriguez, J. Colchero, J. Gomez-Herrero, A. M. Baro, *Rev. Sci. Instrum.* **2007**, *78*, 013705.
[36] P. Giannozzi, et al., *J. Phys.: Condens. Matter* **2009**, *21*, 395502.
[37] J. VandeVondele, M. Krack, F. Mohamed, M. Parrinello, T. Chassaing, J. Hutter, *Comput. Phys. Commun.* **2005**, *167*, 103 – 128.

